Review of Scientific Instruments

An apparatus based on an atomic force microscope for implementing tip-controlled local breakdown

Cite as: Rev. Sci. Instrum. **90**, 123703 (2019); https://doi.org/10.1063/1.5129665
Submitted: 30 September 2019 . Accepted: 30 November 2019 . Published Online: 20 December 2019

T. St-Denis, K. Yazda, X. Capaldi, J. Bustamante, M. Safari, Y. Miyahara, Y. Zhang, P. Grutter, and W. Reisner

AIP Publishing

Review of Scientific Instruments ARTICLE scitation.org/journal/rsi

An apparatus based on an atomic force microscope for implementing tip-controlled local breakdown

Cite as: Rev. Sci. Instrum. 90, 123703 (2019); doi: 10.1063/1.5129665
Submitted: 30 September 2019 • Accepted: 30 November 2019 •
Published Online: 20 December 2019

T. St-Denis,[1] K. Yazda,[1] X. Capaldi,[1] J. Bustamante,[1,2] M. Safari,[3,a)] Y. Miyahara,[1,4,b)] Y. Zhang,[1,5,c)] P. Grutter,[1,d)] and W. Reisner[1,e)]

AFFILIATIONS

[1]Physics Department, McGill University, 3600 rue University, Montreal, Quebec H3A 2T8, Canada
[2]Departamento de Física, Universidad San Francisco de Quito, Quito 170901, Ecuador
[3]Norcada, 4548-99 Street NW, Edmonton, Alberta T6E 5H5, Canada
[4]Department of Physics, Texas State University, 601 University Drive, San Marcos, Texas 78666, USA
[5]BGI-Research, 146 BeiShan Rd., Shenzhen 518083, China

[a)]**Electronic mail:** mojtaba@norcada.com
[b)]**Electronic mail:** yoichi.miyahara@txstate.edu
[c)]**Electronic mail:** zhangyuning@genomics.cn
[d)]**Electronic mail:** peter.grutter@mcgill.ca. **URL:** http://www.physics.mcgill.ca/~peter/.
[e)]**Electronic mail:** reisner@physics.mcgill.ca. **URL:** http://www.physics.mcgill.ca/~reisner/.

ABSTRACT

Solid-state nanopores are powerful tools for sensing of single biomolecules in solution. Fabrication of solid-state nanopores is still challenging, however; in particular, new methods are needed to facilitate the integration of pores with larger nanofluidic and electronic device architectures. We have developed the tip-controlled local breakdown (TCLB) approach, in which an atomic force microscope (AFM) tip is brought into contact with a silicon nitride membrane that is placed onto an electrolyte reservoir. The application of a voltage bias at the AFM tip induces a dielectric breakdown that leads to the formation of a nanopore at the tip position. In this work, we report on the details of the apparatus used to fabricate nanopores using the TCLB method, and we demonstrate the formation of nanopores with smaller, more controlled diameters using a current limiting circuit that zeroes the voltage upon pore formation. Additionally, we demonstrate the capability of TCLB to fabricate pores aligned to embedded topographical features on the membranes.

I. INTRODUCTION

Nanometer scale holes, known as nanopores, are rising in popularity in biological research, as they can be used to detect the passage of single macromolecules.[1–6] When driven by an electric field, charged molecules will thread through nanopores,[7–9] a process known as translocation, inducing a current blockage from which key information about the transport mechanism and the molecule under analysis can be extracted.[10,11] Engineered biological nanopores can be used to read sequences of nucleotides on translocating DNA.[12–18] However, biological nanopores are restrictive due to the limited stability of the lipid support membrane and their fixed diameter.[6] Consequently, there is considerable interest in developing and improving nanopore technology by replacing protein pores with machined holes in silicon nitride membranes and 2D materials like graphene and MoS_2.

In 2001, Li *et al.* developed ion-beam sculpting,[19] the first robust solid-state nanopore formation method. In this approach, a beam of low energy argon ions is used to shrink a large hole initially created via focused-ion beam (FIB), with the pore diameter controlled by monitoring the flow of Ar ions through the pore; the beam is shuttered when the flow-rate falls below a preset value.

Although ion-beam sculpting allows the fabrication of sub-2 nm pores, its lack of precision and control over the internal geometry of pores[20] as well as the development of more efficient techniques led workers to gradually abandon the technique. Storm *et al.* developed a second nanopore fabrication method in 2003 using a transmission electron microscope[21] (TEM). In this approach, the high energy electron beam of the TEM is used to etch pores as small as 0.5 nm in diameter. The adjustable electron beam is used simultaneously for both imaging and etching, which allow precise alignment and control over the nanopore size. A major limitation of the TEM approach is that it requires a freely suspended membrane and cannot form pores on a membrane bonded to a thick device substrate, a limitation that reduces the integration potential of the TEM approach. Another high energy beam technique was developed in 2006 by Lo *et al.* called focused-ion beam (FIB).[22] This approach uses a focused beam of gallium ions to bombard the surface of an insulating membrane until a pore is milled. FIB setups typically include a scanning electron microscope (SEM) that can image the sample surface. This allows the FIB to fabricate pores at specific locations on a membrane by aligning the ion beam with the aid of the SEM. This alignment is mainly required in devices designed to achieve DNA sequencing where a solid-state nanopore is integrated with a microchannel or positioned in between nanoelectrodes.[23–33] However, a major limitation of the FIB method is the difficulty in achieving sub 10 nm pores under standard conditions[20,34,35] without additional steps to alter the sample (e.g., via ion-beam induced deposition post pore formation[36]) or the apparatus (e.g., by adding lenses to focus the ion beam[37]). In 2011, helium ion microscope milling was developed by the Hall Lab[38] to improve the throughput of pore formation of FIB. Nanopores are fabricated by helium ion-beam lithography using a mobile microscope tip capable of creating pore arrays with a throughput close to two pores per minute,[39] with diameter down to 5 nm. Although TEM and FIB are well-established nanopore fabrication techniques, they require expensive equipment, lack scalability, and samples have to be placed in a vacuum. Indeed, the high cost of tools used in these experiments is a significant barrier for anyone entering the nanopore field from the outside.

A distinct fabrication approach termed controlled dielectric breakdown (CBD) was devised by Kwok *et al.*[40,41] In this approach, a voltage pulse is applied across the membrane between otherwise electrically isolated reservoirs. The high voltage induces dielectric breakdown in the membrane, creating a nanopore within seconds. A key disadvantage of the dielectric breakdown approach is that pores are formed at the weakest point of the membrane, making their position essentially random on a surface with low film heterogeneity and flat topography. In addition, the classic CBD approach can create more than one pore, with breakdown happening at more than one weak location.[42] The integration of pores in devices that require precise positioning is thus unfeasible. Recently, techniques localizing the breakdown process to specific regions of the membrane have emerged, by thinning down a specific region of the membrane using an infrared[27] or focused[43] laser, ion-beam milling,[42] or TEM lithography.[44] Although these methods solve the major issue of CBD, they drastically decrease its throughput, as each sample needs to go through additional preparation steps, and increase its cost, since some techniques require the same equipment as FIB or TEM.

To make use of the high scalability and low cost of CBD while maintaining the positioning precision of FIB and TEM, we use a conductive atomic force microscope (AFM) tip to restrict the dielectric breakdown to a single nanoscale region on the membrane. This method, which we call tip-controlled local breakdown[45] (TCLB), requires the AFM tip to be placed in contact with the membrane and then a voltage pulse to be applied across the membrane between AFM tip (in air) and an underlying electrolyte solution. Since current only flows through the region in contact with the tip (with a ~10 nm radius of curvature), an individual nanopore can be created with nanometer precision and multiple nanopore formation is avoided. Also, using the AFM imaging capabilities, pores can be aligned with existing membrane features, facilitating pore integration with other micro and nanoscale elements (e.g., tunneling electrodes, nanochannels, chemically patterned regions).

To improve the control over the pore diameter and to reliably achieve sub-5 nm pores, we designed an Arduino-based circuit that regulates the voltage pulse used to create the nanopores. By interrupting the voltage applied to the membrane immediately after the pore is formed, we have successfully created nanopores half the size of those fabricated in the absence of the circuit (with other conditions kept fixed). This is beneficial as smaller pores improve signal-to-noise, reduce folding, and slow down translocation of biomolecules. We have also demonstrated the integration capability of TCLB by creating nanopores inside 5 μm silicon nitride microwells etched into silicon nitride membranes with an additional oxide layer for capacitive noise reduction.

II. EXPERIMENTAL DESIGN

A. Fabrication setup

A view of the atomic force microscope used in the experiment and a detailed schematic of the setup are provided in Figs. 1(a) and 1(d), respectively. A diamond-coated conductive tip (Adama Innovations, model AD-2.8-AS) is mounted on a Multimode Nanoscope III AFM from Digital Instrument (now Bruker), as shown in Figs. 1(b) and 1(c). The tip is brought in contact with a silicon nitride membrane (the details of the sample used are further discussed in Sec. II B), which is placed on an AS 130VLR-2 scanner (Bruker). The AFM is operated using a Nanoscope IIIa Scanning Probe Microscope Controller in contact mode and measurements of the tip height and deflection are obtained via the Nanoscope Signal Access Module. The tip is aligned on the sample using two monoculars of resolution 10 × 30 (Specwell) located above and in front of the AFM head. Once the membrane has been located and the tip is positioned onto it, we execute a script to send a rectangular voltage pulse (of fixed amplitude and width predetermined based on membrane thickness) to the tip. The pulse voltage is generated by the Nanoscope controller and amplified by a home-built voltage amplifier. A current probing wire is attached to the sample holder disk, and the wire is connected to a custom built I-V converter with transimpedance gain of 10^9. The output of the I-V converter is used to confirm successful pore formation. A quad-channel oscilloscope (Picoscope 4444 from Pico Technologies) is used to record the tip voltage pulse and current, sample's vertical position, and cantilever's deflection. The AFM sits on an active vibration

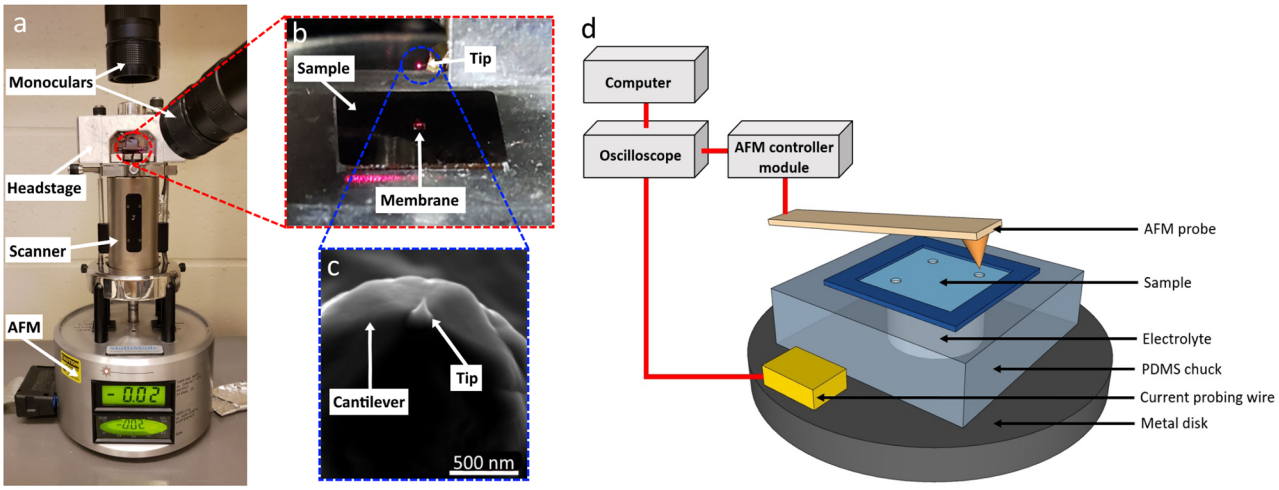

FIG. 1. Setup used to fabricate nanopores using TCLB. (a) The AFM setup used: the sample is placed on top of the AFM scanner. Two monoculars are used to carefully align the tip with the membrane. (b) Magnified view of the sample holder, where the tip is shown above the sample membrane. (c) SEM image of the AFM tip. (d) Sketch of the sample and schematic of the apparatus. The AFM is used to make multiple pores on the sample membrane, which sits on top of and is in contact with the electrolyte solution. The solution is also in contact with a metal disk at the bottom of the chuck so that current flows through the membrane when the pulse is applied at the tip. A current probing wire is magnetically attached to the disk. The Nanoscope console (AFM controller module) is used to measure the tip voltage, height, and deflection. The current probing wire is connected to a custom build I-V converter, and its output is connected to the Picoscope oscilloscope.

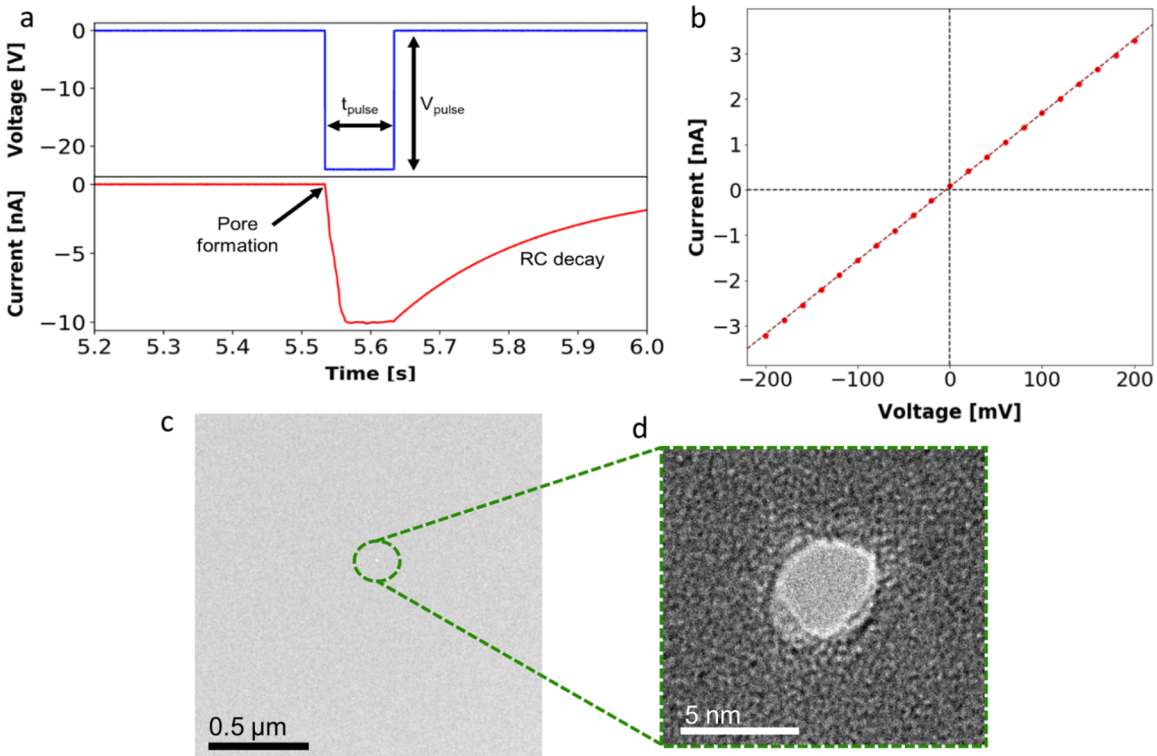

FIG. 2. Different methods of detecting nanopores. (a) Graphs of the voltage pulse and the corresponding current drop across the membrane recorded by the Picoscope oscilloscope. A pulse of −24 V was applied for 100 ms on a 15 nm thick silicon nitride membrane. We can observe a small delay between the voltage and current drops, corresponding to the breakdown time, after which the pore is formed. Applying voltage past that point only serves to increase the pore size. (b) I-V curve of the same nanopore. The conductance of the pore, represented by the slope of the graph, is 16.23 nS, which corresponds to a pore size of 7.9 nm [obtained by using Eq (1)]. (c) TEM micrograph of a different 15 nm thick silicon nitride membrane containing a 4.5 nm nanopore. (d) Magnified TEM micrograph of the same pore.

isolation system (TS-150 Herzan) to minimize noise when performing scans.

To create nanopores, we first image the sample with the tip to locate the membrane using the NanoScope software. Once the membrane has been located, we align the field of view of the AFM at the position where the pores need to be created. Using the Nanoscope software, we then execute a script written with the Nanoscript package (Bruker) to position the tip at the desired location and to engage it with the surface. In this script, we set the amplitude of the voltage pulse, V_{pulse}, and its width duration, t_{pulse}, depending on the membrane used. Also, using a set of for-loops, we can automatically change the position of the tip during the pore formation stage, thus allowing the formation of pore arrays of variable spacing (we use a spacing of 500 nm). Furthermore, we are able to use different V_{pulse} and t_{pulse} values for each column of the nanopore arrays in order to quantify the pore formation process based on varying conditions within a single experiment.

B. Sample preparation

The thin membrane samples consist of a silicon frame surrounding a free-standing silicon nitride (SiN_x) membrane (Norcada, part number NBPT005YZ-HR and NT002Y). Nanopores can be made in membranes of different thicknesses, though the voltage required to induce a dielectric breakdown in the membrane will depend on its thickness. The experiment is performed under ambient laboratory conditions, and only one side of the membrane needs to be in contact with the electrolyte reservoir. A chuck made from a polydimethylsiloxane (PDMS) square adhered to a magnetic stainless steel disk is used to hold the sample [Fig. 1(b)]. A hole punctured through the PDMS is used to hold the electrolyte solution (consisting of 1 M sodium perchlorate dissolved in propylene carbonate, with 2.82 S m^{-1} of conductivity). The membrane is exposed to O_2 plasma for 45 s to ensure complete wetting of the membrane's bottom side. Then, the sample is placed onto the chuck such that the membrane is in contact with the electrolyte reservoir. The

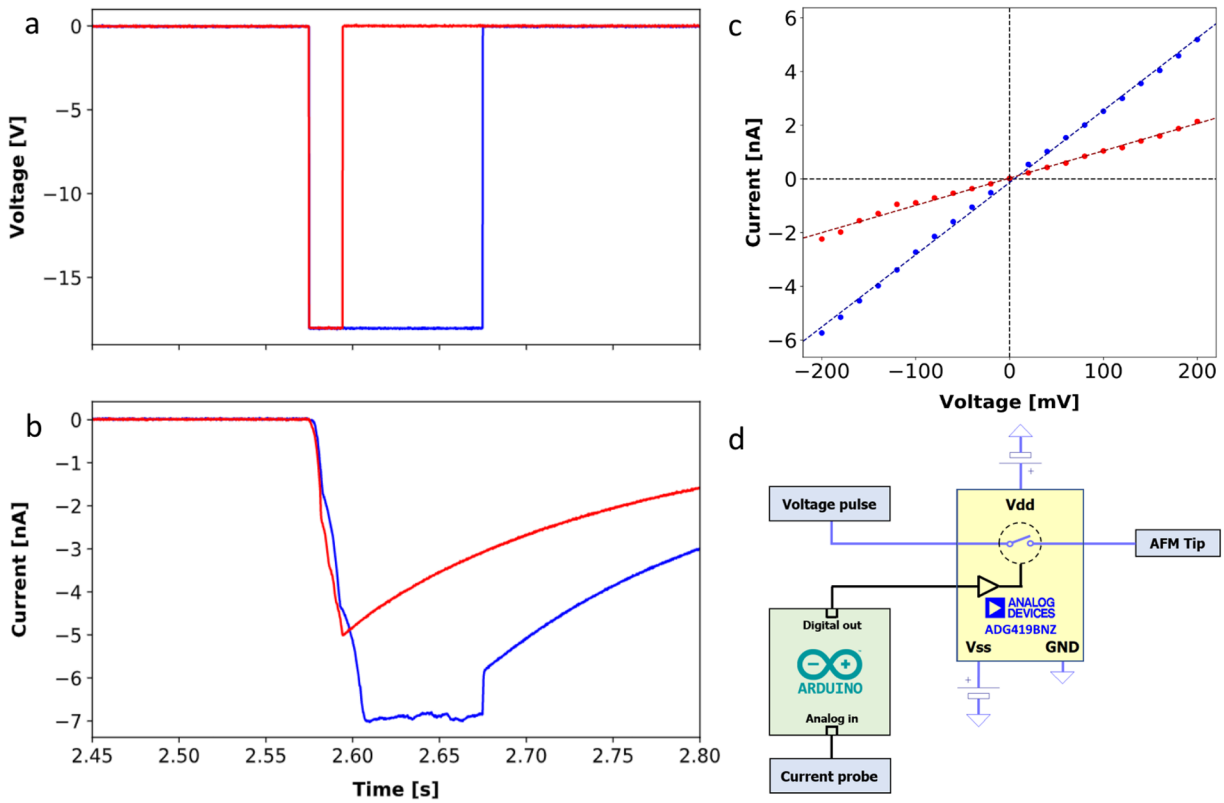

FIG. 3. Graphs of (a) the voltage pulse and (b) the corresponding current drop across the membrane recorded by the Picoscope oscilloscope. A pulse of −18 V was applied for 100 ms on a 12 nm thick silicon nitride membrane. The blue curves correspond to the pore created with the passive system; the red curves were obtained using the active system with a current threshold value of −5 nA. Note the absence of a long current plateau in the active approach, indicating the reduction of current flow through the pore vis-a-vis the passive approach. In both cases, we can observe a small delay between the voltage and current drops, corresponding to the breakdown time. (c) I-V curves for nanopores corresponding to the breakdown curves shown in subfigures (a) and (b). The conductance of the passive system pore is 26.88 nS, which yields a pore size of 9.8 nm, whereas the conductance of the active system pore is 10.16 nS, from which we obtain a diameter of 5.5 nm. (d) Schematic circuit drawing of the Arduino-based active current cutoff system. The current probe reading the *trans*-pore current is then connected to the Arduino, which controls the switch (Analog Devices, Inc., ADG419BNZ) that connects the voltage pulse to the AFM tip. Once a preset limiting current threshold is reached, the Arduino opens the switch and zeroes the voltage drop across the membrane.

current probing wire is attached magnetically to the chuck's metal disk.

C. Nanopore detection methods

Once a voltage pulse is applied to the membrane, a dielectric breakdown process is initiated on the membrane. Successful pore formation is indicated by an increase in current magnitude, which rapidly increases at the moment of pore formation and then stays constant for the remaining duration of the pulse [Fig. 2(a)].

Furthermore, if the diameter of the nanopore is bigger than the tip radius of the AFM, we can directly image the pore with a topological scan using the AFM. Alternatively, a liquid spill can sometimes be observed during a scan, which is the result of the electrolyte solution overflowing through a pore, thus confirming the presence of a nanopore. A TEM can also be used to obtain an image of smaller pores, which allows us to further confirm a successful fabrication process and to determine the pore shape and location (Fig. 2).

The pore diameter can be determined by measuring the I-V curve for the pore [Fig. 2(b)]. The I-V curve of the pore is obtained by placing the membrane in a 3D printed chuck with KCl-filled buffer reservoirs accessing the top and bottom of the pore. A patch-clamp amplifier (Molecular Devices, Axopatch 200B) is then used to measure the *trans*-pore current as the voltage is varied, which gives access to the nanopore conductance. The nanopore diameter is related to pore conductance via the following equation:[46]

$$G = \sigma\left(\frac{4l}{\pi d^2} + \frac{1}{d}\right)^{-1}, \tag{1}$$

where σ is the membrane bulk conductivity, l is the membrane thickness, and d is the pore diameter. We can solve for d to obtain the diameter of the pore directly from the conductance.

III. CHARACTERIZATION AND PERFORMANCE

A. Current limiting systems

Applying voltage past the point of pore formation only serves to increase the pore diameter. Consequently, we have developed two approaches for limiting the current once a pore is formed.[47] The first approach is a passive current limiting circuit consisting of a 2 GΩ resistor placed in series with the current probing wire. This resistance value has been chosen to be much smaller than the membrane's innate resistance prior to pore formation, but larger than its resistance after pore formation. This arrangement, effectively a simple voltage divider, greatly reduces the voltage dropped across the membrane once the resistance of the membrane (falling due to the formation of the pore) drops below 2 GΩ. However, the passive current limiting circuit does not completely prevent current flow across the membrane. Completely halting the current flow is essential to prevent any inadvertent increase in the pore size and achieve the smallest possible pores (as well as gain more fine control over the resulting diameter). To ensure more controlled current flow, we have developed an active current limiting circuit using an Arduino Due microcontroller. This active current limiting approach is designed to completely cut-off the current flow across the pore once a certain current threshold is reached. The resulting pore size can be varied by adjusting the current threshold value. To implement

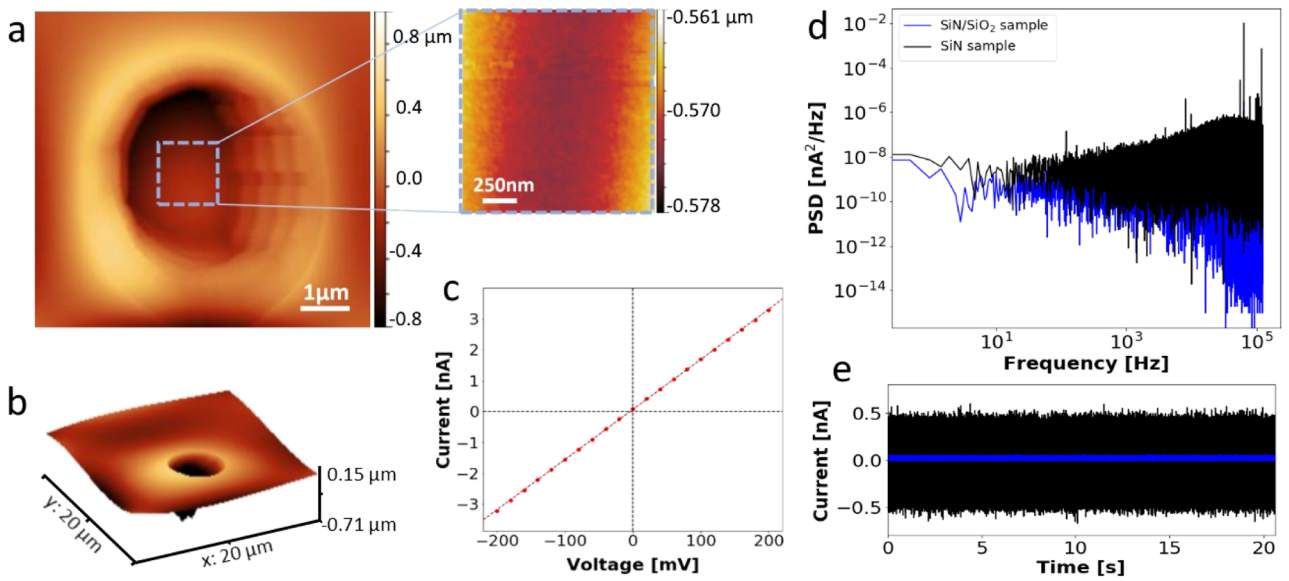

FIG. 4. TCLB applied on a sample with integrated microwell features. (a) Topographic AFM scan of 5 μm diameter microwell containing a 15 nm thick silicon nitride membrane at the well bottom. (b) A 3D representation of the same data as in (a). (c) I-V curve of the nanopore that was fabricated in the microwell, which has a conductance of 16.2 nS resulting in a diameter of 7.7 nm. (d) Current power spectral density plot comparison between two nanopores of similar sizes, with one pore created in a standard 15 nm SiN chip and the other in the SiN/SiO_2 sample with 15 nm microwell. This was obtained by applying 200 mV through the pore and measuring the resulting 100 kHz low-pass filtered ionic current trace for 10 s at 250 kHz sampling rate. (e) Baseline measurements of the two same pores. The noise analysis reveals that the oxide layer provides an increase in signal-to-noise by ~2 orders of magnitude, which greatly improves the quality of results of DNA translocation experiments.

the active approach, we connect the analog input of the Arduino to the current probing wire and the digital output to the logic input of an analog switch (Analog Devices, Inc., ADG419BNZ). The analog switch, with its on or off state determined by the Arduino's logic input, is used to supply the voltage pulse to the AFM tip [as shown in Fig. 3(d)]. When the current level rises above a preset threshold, the switch opens the circuit within microseconds, halting current flow and preventing further increase in the pore size. Note that using the Arduino alone to produce the voltage pulse introduces too much noise, especially since the signal it provides needs to be amplified.

To benchmark the performance of the passive current limiting and active cutoff circuit approaches, we have created nanopores in 12 nm thick silicon nitride samples, using both approaches [see Figs. 3(a) and 3(b) for examples of both approaches]. We can see that in the case of the active system, once the current threshold value set beforehand in the Arduino code is reached, the voltage pulse is immediately zeroed, which happens within a few milliseconds, whereas the other pulse lasts the full 100 ms. By analyzing the I-V curves of both samples [Fig. 3(c)], we obtain a difference in the pore diameter of 4.3 nm between the two systems, where the pore created with the active circuit is about half the size (56% smaller) than that formed with the passive circuit. This supports the claim that pores grow in size as they are continuously fed with current and indicates that the active system can indeed be used to fabricate smaller pores.

B. Device integration of TCLB nanopores

A powerful feature of the TCLB technique is that the AFM's imaging capabilities can be used to align nanopores to pre-existing features on a membrane. For example, the AFM's topographical scanning capabilities can be used to identify regions of the membrane, which are locally etched or contain deposited materials. Then, we can move the tip position or further zoom in on specific regions of the surface until the desired location for pore fabrication has been located. To support this claim, we used TCLB to create a pore at the floor of a microwell structure. In particular, we used NBPT004YZ-00-5umW-LR devices (provided by Norcada) that consist of a 35 μm × 35 μm SiO_2/SiN_x window containing a 5 μm diameter SiN_x microwell. To fabricate the microwell, the multistack of SiO_2/SiN_x is patterned and etched, resulting in a 15 nm thick SiN_x membrane at the bottom of the microwell [as shown in Figs. 4(a) and 4(b)]. We then used TCLB to create a 7.7 nm of the diameter pore [Fig. 4(c)]. The addition of the oxide layer lowers the capacitive noise. Figure 4(d) shows an increase by ~2 orders of magnitude in the signal-to-noise ratio obtained using these SiO_2/SiN_x samples compared to samples exclusively made of silicon nitride.

IV. CONCLUSIONS

In summary, we have developed a scalable and inexpensive technique capable of creating solid-state nanopores in thin, insulating membranes. This is achieved by inducing a dielectric breakdown in a local region via a voltage pulse applied at an AFM tip. An Arduino-based control circuit was added to the apparatus to zero the voltage pulse microseconds after pore formation, resulting in smaller, more controlled pore diameters. With the use of the imaging capabilities of the AFM, we are able to align pores to pre-existing features on the membranes, such as microwells. Also, these samples contained a layer of silicon oxide, which yielded a remarkable reduction in signal-to-noise levels compared with standard silicon nitride membranes. This offers a promising prospect for genomics applications as one of the main obstacles preventing DNA sequencing via solid-state nanopores using ionic current analysis is its high background noise level.

ACKNOWLEDGMENTS

This work was financially supported by the Natural Sciences and Engineering Research Council of Canada (NSERC) Discovery Grants Program (Grant Nos. RGPIN 386212 and RGPIN 05033), Idea to Innovation (I2I) Grant (No. I2IPJ 520635-18), joint CIHR funded Canadian Health Research Projects Grant (No. CIHRR CPG-140199), and the Fonds de Recherche du Québec Nature et Technologie (FRQNT) funded Regroupement Québécois sur les Matériaux de Pointe (RQMP). The authors acknowledge Norcada for material supplies (ultrathin membranes) and MEMS device design collaboration.

REFERENCES

[1] M. Wanunu, Phys. Life Rev. **9**, 125 (2012).
[2] J. J. Kasianowicz, J. W. Robertson, E. R. Chan, J. E. Reiner, and V. M. Stanford, Annu. Rev. Anal. Chem. **1**, 737 (2008).
[3] B. M. Venkatesan and R. Bashir, Nat. Nanotechnol. **6**, 615 (2011).
[4] B. Sakmann and E. Neher, *Single-Channel Recording* (Springer, 1995).
[5] D. Branton, D. W. Deamer, A. Marziali, H. Bayley, S. A. Benner, T. Butler, M. Di Ventra, S. Garaj, A. Hibbs, X. Huang, S. B. Jovanovich, P. S. Krstic, S. Lindsay, X. S. Ling, C. H. Mastrangelo, A. Meller, J. S. Oliver, Y. V. Pershin, J. M. Ramsey, R. Riehn, G. V. Soni, V. Tabard-Cossa, M. Wanunu, M. Wiggin, and J. A. Schloss, Nat. Biotechnol. **26**, 1146 (2008).
[6] C. Dekker, Nat. Nanotechnol. **2**, 209 (2007).
[7] Z. Yuan, A. L. Garcia, G. P. Lopez, and D. N. Petsev, Electrophoresis **28**, 595 (2007).
[8] R. B. Schoch, J. Han, and P. Renaud, Rev. Mod. Phys. **80**, 839 (2008).
[9] W. Sparreboom, A. Van den Berg, and J. C. T. Eijkel, New J. Phys. **12**, 015004 (2010).
[10] S. Lindsay, Nat. Nanotechnol. **11**, 109 (2016).
[11] J. Clarke, H.-C. Wu, L. Jayasinghe, A. Patel, S. Reid, and H. Bayley, Nat. Nanotechnol. **4**, 265 (2009).
[12] J. J. Kasianowicz, E. Brandin, D. Branton, and D. W. Deamer, Proc. Natl. Acad. Sci. U. S. A. **93**, 13770 (1996).
[13] L.-Q. Gu, O. Braha, S. Conlan, S. Cheley, and H. Bayley, Nature **398**, 686 (1999).
[14] S. Howorka, S. Cheley, and H. Bayley, Nat. Biotechnol. **19**, 636 (2001).
[15] A. Meller, L. Nivon, and D. Branton, Phys. Rev. Lett. **86**, 3435 (2001).
[16] I. M. Derrington, T. Z. Butler, M. D. Collins, E. Manrao, M. Pavlenok, M. Niederweis, and J. H. Gundlach, Proc. Natl. Acad. Sci. U. S. A. **107**, 16060 (2010).
[17] G. F. Schneider and C. Dekker, Nat. Biotechnol. **30**, 326 (2012).
[18] F. Yanxiao, Z. Yuechuan, Y. Cuifeng, W. Deqiang, and D. Chunlei, Genomics, Proteomics Bioinf. **13**, 4 (2015).
[19] J. Li, D. Stein, C. McMullan, D. Branton, M. J. Aziz, and J. A. Golovchenko, Nature **412**, 166 (2001).
[20] A. T. Kuan and J. A. Golovchenko, Appl. Phys. Lett. **100**, 213104 (2012).
[21] A. J. Storm, J. H. Chen, X. S. Ling, H. W. Zandbergen, and C. Dekker, Nat. Mater. **2**, 537 (2003).
[22] C. J. Lo, T. Aref, and A. Bezryadin, Nanotechnology **17**, 3264 (2006).

[23]B. Gierhart, D. Howitt, S. Chen, Z. Zhu, D. Kotecki, R. Smith, and S. Collins, Sens. Actuators, B **132**, 593 (2008).
[24]A. P. Ivanov, E. Instuli, C. M. McGilvery, G. Baldwin, D. W. McComb, T. Albrecht, and J. B. Edel, Nano Lett. **11**, 279 (2011).
[25]M. P. Jonsson and C. Dekker, Nano Lett. **13**, 1029 (2013).
[26]F. Nicoli, D. Verschueren, M. Klein, C. Dekker, and M. P. Jonsson, Nano Lett. **14**, 6917 (2014).
[27]S. Pud, D. Verschueren, N. Vukovic, C. Plesa, M. P. Jonsson, and C. Dekker, Nano Lett. **15**, 7112 (2015).
[28]M. Belkin, S.-H. Chao, M. P. Jonsson, C. Dekker, and A. Aksimentiev, ACS Nano **9**, 10598 (2015).
[29]X. Shi, D. Verschueren, S. Pud, and C. Dekker, Small **14**, 1703307 (2018).
[30]Y. Zhang and W. Reisner, Nanotechnology **26**, 455301 (2015).
[31]Y. Zhang, X. Liu, Y. Zhao, J.-K. Yu, W. Reisner, and W. B. Dunbar, Small **14**, 1801890 (2018).
[32]X. Liu, Y. Zhang, R. Nagel, W. Reisner, and W. B. Dunbar, Small **15**, 1901704 (2019).
[33]R. Tahvildari, E. Beamish, V. Tabard-Cossa, and M. Godin, Lab Chip **15**, 1407 (2015).
[34]B. N. Miles, A. P. Ivanov, K. A. Wilson, F. Doğan, D. Japrung, and J. B. Edel, Chem. Soc. Rev. **42**, 15 (2013).
[35]C. Wen, S. Zeng, K. Arstila, T. Sajavaara, Y. Zhu, Z. Zhang, and S.-L. Zhang, Am. Chem. Soc. **2**, 300 (2017).
[36]J. Nilsson, J. Lee, T. Ratto, and S. Létant, Adv. Mater. **18**, 427 (2006).
[37]J. Gierak, A. Madouri, A. Biance, E. Bourhis, G. Patriarche, C. Ulysse, D. Lucot, X. Lafosse, L. Auvray, L. Bruchhaus, and R. Jede, Microelectron. Eng. **84**, 779 (2007).
[38]J. Yang, D. C. Ferranti, L. A. Stern, C. A. Sanford, J. Huang, Z. Ren, L.-C. Qin, and A. R. Hall, Nanotechnology **22**, 285310 (2011).
[39]D. Xia, C. Huynh, S. McVey, A. Kobler, L. Stern, Z. Yuan, and X. S. Ling, Nanoscale **10**, 5198 (2018).
[40]H. Kwok, K. Briggs, and V. Tabard-Cossa, PLoS One **9**, 1 (2014).
[41]K. Briggs, H. Kwok, and V. Tabard-Cossa, Small **10**, 2077 (2014).
[42]A. Zrehen, T. Gilboa, and A. Meller, Nanoscale **9**, 16437 (2017).
[43]T. Gilboa, A. Zrehen, A. Girsault, and A. Meller, Sci. Rep. **8**, 9765 (2018).
[44]A. T. Carlsen, K. Briggs, A. R. Hall, and V. Tabard-Cossa, Nanotechnology **28**, 085304 (2017).
[45]Y. Zhang, Y. Miyahara, N. Derriche, W. Yang, K. Yazda, X. Capaldi, Z. Liu, P. Grutter, and W. Reisner, Small Methods **3**, 1900147 (2019).
[46]S. W. Kowalczyk, A. Y. Grosberg, Y. Rabin, and C. Dekker, Nanotechnology **22**, 315101 (2011).
[47]E. Beamish, H. Kwok, V. Tabard-Cossa, and M. Godin, Nanotechnology **23**, 405301 (2012).